High-efficiency, continuous-wave Fe:ZnSe mid-IR laser end pumped by an Er:YAP laser

doi: https://doi.org/10.1364/OE.444625

Research Article | Vol. 29, No. 26 / 20 Dec 2021 / Optics Express 44118
Optics EXPRESS

High-efficiency, continuous-wave Fe:ZnSe mid-IR laser end pumped by an Er:YAP laser

ENHAO LI,[1] HIYORI UEHARA,[1,2] WEICHAO YAO,[2] SHIGEKI TOKITA,[3] FEDOR POTEMKIN,[4] AND RYO YASUHARA[1,2,*]

[1]The Graduate University for Advanced Studies, SOKENDAI, 322-6, Oroshi-cho, Toki 509-5292, Japan
[2]National Institute for Fusion Science, 322-6, Oroshi-cho, Toki 509-5292, Japan
[3]Institute of Laser Engineering, Osaka University, 2-6 Yamada-oka, Suita, Osaka 565-0871, Japan
[4]M.V. Lomonosov Moscow State University, Leninskie Gory, bld. 1/62, Moscow 119991, Russia
*yasuhara@nifs.ac.jp

Abstract: Fe:ZnSe lasers operating in the mid-IR spectral region have gained widespread attention due to their numerous potential applications. This study presents a high-efficiency, continuous-wave Fe:ZnSe laser end pumped by an Er:YAP laser at 2920 nm. The Er:YAP laser was home-constructed and generated an output power of 3.6 W and an average slope efficiency of 36.6% with a good beam quality ($M^2 \leq 2$). The Fe:ZnSe laser produced a maximum output power of 1 W at 4.06 μm for 2.1 W of absorbed pump power, corresponding to an average slope efficiency of 48%. Theoretical modeling of the continuous-wave Fe:ZnSe laser is presented to determine the prospects for further power scaling.

1. Introduction

Mid-IR lasers based on transition metal-doped II-IV chalcogenides (e.g., Cr:ZnS, Cr:ZnSe, Fe:ZnS, Fe:ZnSe, etc.) have gained widespread attention over the past decade [1], primarily due to their numerous potential applications in remote sensing, molecular spectroscopy, LIDAR, and space communication [2–4]. The transition metal-doped II-IV chalcogenides exhibit significant broad absorption and emission bands as well as large cross sections owing to the small energy splitting and strong electron-phonon coupling of transition metal ions in tetrahedral coordination, making them well-suited for the generation of mid-IR tunable lasers and ultrafast lasers. Particularly, Fe:ZnSe has been extensively analyzed for generating 3.8-5.2 μm radiation owing to its longer fluorescence lifetime when compared to Fe:ZnS and Fe:CdSe. Hitherto, various modes of operation, including free-running [5,6], gain-switching [7,8], continuous-wave (CW) [9], Q-switching [10–12] and mode-locking [13] with Fe:ZnSe single crystals or polycrystals have been widely studied and reported.

However, the development of the CW Fe:ZnSe lasers has remained limited despite the impressive laser performance presented by Fe:ZnSe due to the lack of reliable 3 μm CW pump sources with high output power and good beam quality, along with the high requirements for cumbersome cryogenic cooling systems. Thus far, only a few high performance 3 μm lasers have been developed for pumping the CW Fe:ZnSe lasers, which are primarily based on chromium-doped chalcogenides (Cr:CdSe, Cr:ZnSe) and on rare-earth erbium-doped crystals or fibers (Er:YAG, Er:Y_2O_3, Er:ZBLAN) [9,14–17]. The highest output power reported for the CW Fe:ZnSe lasers was achieved by employing a Cr:ZnSe laser as the pump source, which produced 9.2 W of output power with an optical-to-optical efficiency of 40% [16]. Recently, the Er:ZBLAN fiber laser has emerged as a promising pump source for the Fe:ZnSe laser, which presented 2.1 W of Fe:ZnSe output power with 59% of slope efficiency [17]. The Cr:ZnSe laser and the Er:ZBLAN fiber laser remain limited despite their excellent performance, as they require significant thermal management and elaborate design to prevent damage to the gain elements [18,19]. A diode-pumped Er:$YAlO_3$ (Er:YAP) laser, which has been developed recently based

#444625 https://doi.org/10.1364/OE.444625
Journal © 2021 Received 29 Sep 2021; revised 12 Nov 2021; accepted 13 Nov 2021; published 16 Dec 2021

Optics EXPRESS

on a simple and compact two-mirror cavity design, was able to generate nearly 7 W of output power [20], demonstrating the potential of the Er:YAP crystal in the power scaling of 3 μm lasers. The Er:YAP crystal possesses a lower thermo-optic coefficient than the Cr:ZnSe crystal and a more robust mechanical property than the Er:ZBLAN fiber, indicating the low requirements for thermal managements. Additionally, the lasing wavelength of the Er:YAP crystal was stabilized at 2920 nm, presenting a higher quantum efficiency and a higher pump absorption for pumping the Fe:ZnSe laser when compared to the Er:ZBLAN laser (typically emitting at 2800 nm [17]). The high performance, robustness, and low cost of the Er:YAP laser indicate its considerable potential for the pumping of the Fe:ZnSe laser.

This paper presents the novel development of a CW Fe:ZnSe laser end pumped by a self-constructed Er:YAP laser operating at 2920 nm. Detailed lasing characteristics of the output power, spectra, and beam quality are studied for both the Er:YAP pump source and the Fe:ZnSe laser. A rate equation model is also presented to evaluate the laser performance of the CW Fe:ZnSe laser. The calculated results are comprehensively compared with our experimental results to determine the validity of the proposed model. Additionally, thermal analysis of the cryogenically cooled Fe:ZnSe laser is conducted using finite element analysis, for the first time based on our knowledge.

2. Experimental setup

A continuous-wave Er:YAP laser was designed to pump the Fe:ZnSe laser, as shown in Fig. 1(a). A fiber-coupled laser diode with a stabilized central wavelength of 976.2 nm and a linewidth of 0.1 nm was used to pump the Er:YAP crystal. The use of a wavelength-stabilized laser diode was to mitigate the possible excited-state absorption ($^4I_{11/2} \rightarrow {}^4F_{7/2}$) of the Er:YAP crystal [21] and to ensure high stability during laser operation. The coupling fiber had a core diameter of 105 μm and a numerical aperture of 0.22. The output from the laser diode was collimated by a 20 mm focal-length aspheric lens and was then focused to a beam waist radius of ~260 μm by a plano-convex lens of 100-mm focal length. The relatively larger pump size, when compared to the system in [20], was selected to mitigate the thermal lensing effects and thus achieve a higher beam quality at high power levels.

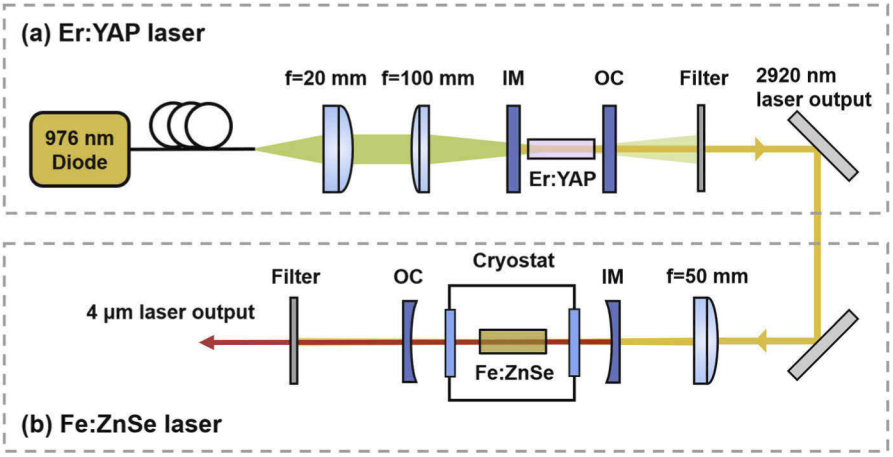

Fig. 1. Experimental setup of Fe:ZnSe laser pumped by Er:YAP laser. (a) Er:YAP laser. (b) Fe:ZnSe laser. IM: input mirror; OC: output coupler.

The Er:YAP laser design was based on a compact plane-plane cavity configuration, comprising a plane input mirror coated for high transmission (T>97%) at the pump wavelength of ~976 nm

Optics EXPRESS

and high reflection (R>99%) at the lasing wavelength of ~2.9 μm, an uncoated b-cut Er:YAP crystal (space group: *Pbnm*), and a plane output coupler with a transmission of 2.5% at ~2.9 μm. The Er:YAP crystal with a doping concentration of 5 at.% was slab-shaped, with a cross-sectional area of 2 mm×5 mm and a length of 8 mm. The crystal was mounted with a 50 μm thick indium foil encased in a well-designed copper heat sink, which was water-cooled to 16 °C. The resonator was kept as short as possible to minimize intracavity loss and to ensure stability during high-power operation. A bandpass filter (2.5-3.1 μm) was placed behind the resonator to separate the laser output from the residual pump light.

Figure 2(a) shows the output power of the Er:YAP laser as a function of the absorbed pump power. The Er:YAP crystal absorbed approximately 71% of the incident pump power. A maximum laser output power of 3.6 W was obtained at the absorbed pump power of 11.4 W, with a corresponding average slope efficiency of 36.6%. The slope efficiency higher than the Stokes limit (33.4%) can be attributed to the effective energy transfer up-conversion process ($^4I_{13/2} + {}^4I_{13/2} \rightarrow {}^4I_{9/2} + {}^4I_{15/2}$) in the Er laser systems [22], which could recycle population of the lower laser level to the upper laser level and thus increase the quantum efficiency. The lasing wavelength was centered at 2920.8 nm with a spectral linewidth of 0.2 nm (see the inset of Fig. 2(a)). Compared to the lasing wavelengths of ~2.7 μm reported in [23], the proposed Er:YAP laser was stabilized at 2920 nm at the output power of over 100 mW, which was attributed to the population accumulation of the lower laser level ($^4I_{13/2}$) at high pump intensities as well as the specific coating property of the output coupler. The power fluctuation at the highest output power was less than 3%. Notably, a higher output power can be achieved with further increase in the pump power [20], but at the risk of higher power instability, degradation in beam quality, and even crystal damage. Therefore, the output power of the Er:YAP laser was not further increased in the subsequent Fe:ZnSe laser experiment. The beam quality at the maximum output power was measured by using the 90/10 knife-edge method to be M_x^2~2.0 and M_y^2~1.8, as shown in Fig. 2(b).

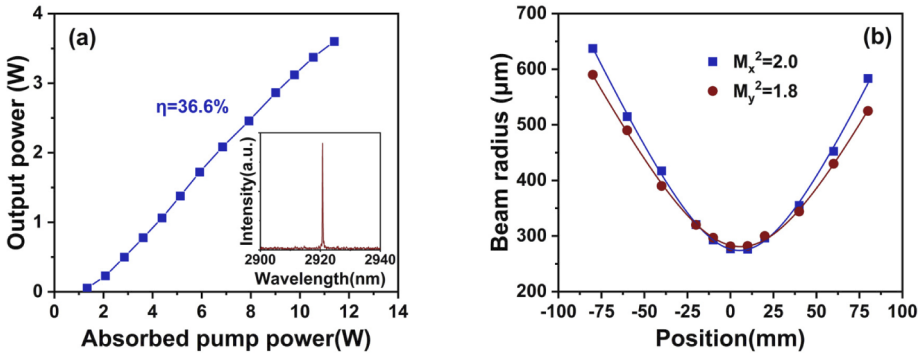

Fig. 2. (a) Er:YAP laser output power versus absorbed pump power. Inset: laser spectrum. (b) Beam quality measurement with 90/10 knife-edge method at maximum output power.

A compact linear resonator was employed for the Fe:ZnSe laser (see Fig. 1(b)), which consisted of a 100 mm radius-of-curvature input mirror coated for high transmission (T>95%) at ~2.9 μm and high reflection (R>99%) at 3.8-5.1 μm, and a 100 mm radius-of-curvature output coupler. Three output couplers (T=2.5%, 10%, and 20%) were used to comprehensively analyze the laser performance. The Fe:ZnSe single crystal was grown from a vapor phase using the seeded physical vapor transport technique by the Lebedev Physical Institute of the Russian Academy of Science [24]. The crystal had a cross-sectional area of 2 mm×4 mm and a length of 8 mm; both the end facets were anti-reflection coated at the pump and lasing wavelengths. The doping concentration was determined to be ~2.2×10^{18} cm^{-3} according to the small signal absorption

Optics EXPRESS

measured at room temperature. The Fe:ZnSe crystal was mounted in a 10 mm long cryostat and was cryogenically cooled to 77 K by liquid nitrogen. The two windows of the cryostat were made of BaF_2 which was anti-reflection coated at 2-5 μm. The vacuum chamber was evacuated to a pressure below 1.5 mTorr. The total length of the cavity was approximately 40 mm; thus, the calculated TEM_{00} mode had a radius of ~210 μm. A CaF_2 lens with a focal length of 50 mm was used to focus the output of the Er:YAP laser into the center of the Fe:ZnSe crystal. The pump waist radius was experimentally measured to be ~140 μm after it was passed through the input mirror. This relatively small pump spot size was selected to achieve a large pump power density and a high lasing efficiency. A bandpass filter (3.8-4.2 μm) was placed behind the Fe:ZnSe resonator to block the unabsorbed pump light. The pump coupling efficiency after the Er:YAP laser passing through the 3 μm bandpass filter, CaF_2 lens, input mirror, and BaF_2 window was measured to be 72%, resulting in a maximum pump power of 2.5 W incident upon the Fe:ZnSe crystal.

3. Results and discussion

3.1. Laser performance of Fe:ZnSe laser

The small signal absorption of the Fe:ZnSe single crystal was determined to be ~85% by measuring the unabsorbed pump power that transmitted through the crystal under non-lasing conditions. This small signal absorption value was used to calculate the absorbed pump power as the ground state bleaching can be considerably mitigated under the lasing conditions. The threshold pump power and laser slope efficiency were measured for the three types of output couplers, as shown in Fig. 3(a). The threshold pump power for the output couplers with T=2.5%, T=10%, and T=20% were 88 mW, 104 mW, and 153 mW, respectively, and the corresponding slope efficiencies with respect to the absorbed pump power were 10.8%, 30.8%, and 46.1%, respectively. Thus, the total intracavity loss coefficient was calculated to be 0.13 cm^{-1} according to the Findlay-Clay method [25]. This internal loss was primarily attributed to the imperfect anti-reflection coating of the two BaF_2 windows and the Fe:ZnSe crystal. A larger output coupling transmission of 20% was preferred for higher lasing efficiency and output power owing to the high gain of the Fe:ZnSe crystal. A maximum output power of ~1 W was obtained at the maximum absorbed pump power of 2.1 W, as shown in Fig. 3(b). The average slope efficiency and the optical-to-optical efficiency were 48% and 40%, respectively. The overall optical conversion efficiency, calculated from the 976 nm diode laser to the 4 μm Fe:ZnSe laser, was 8.8%, which is assumed to represent the highest conversion efficiency for the CW Fe:ZnSe laser reported thus far.

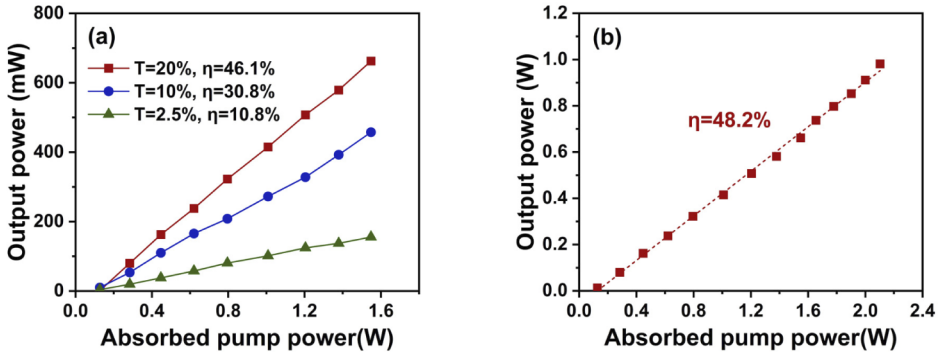

Fig. 3. (a) Fe:ZnSe laser output power versus absorbed pump power with three output couplers. (b) Power scaling performance of Fe:ZnSe laser.

Optics EXPRESS

The emission spectra of the Fe:ZnSe laser were recorded using a spectrum analyzer (771B-MIR, Bristol Instruments) with a spectral resolution of 0.1 nm. Figure 4(a) illustrates the typical lasing spectra for output couplers with T=2.5%, T=10%, and T=20%, recorded at an output power of ~200 mW, demonstrating a broadband multi-spike structure. A slight blue shift was observed in the central lasing wavelength with the increase in the output transmission, which was attributed to the decreased reabsorption loss induced by a high population inversion ratio. Figure 4(b) depicts the variations in the lasing central wavelength and wavelength span with the output power for T=20%. The central wavelength shifted from 4012 nm to 4057 nm with the increase in the output power, and the lasing wavelength span increased from 35 nm to 115 nm. The changes in the central wavelength were primarily attributed to the localized temperature increase of the Fe:ZnSe crystal inside the pumping region, causing a redistribution of population among the energy levels of the Fe ions and the subsequent increase of reabsorption loss at shorter wavelengths. Additionally, the temperature rise would also result in the broadening of the emission spectrum of Fe:ZnSe [26], which is one of the reasons for the increase in the wavelength span.

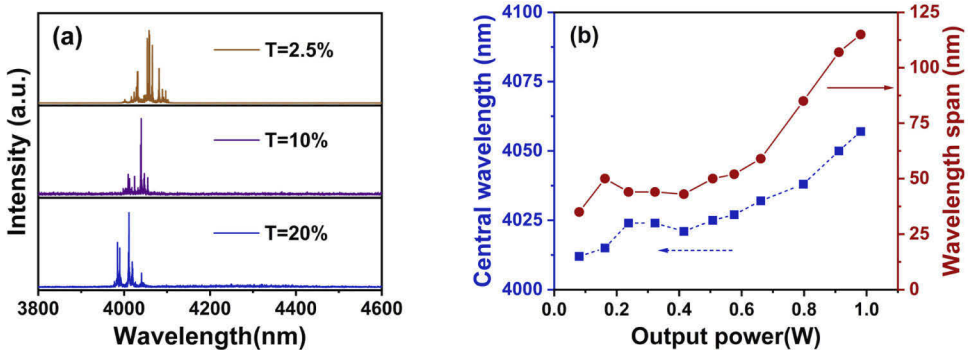

Fig. 4. (a) Typical lasing spectra for output couplers of T=2.5%, 10% and 20%. (b) Lasing central wavelength and wavelength span versus output power of Fe:ZnSe laser.

The beam quality was characterized by using the 90/10 knife-edge method. A CaF_2 lens with a focal length of 100 mm was used to focus the laser output to measure the beam radii along the propagation path. The beam quality factor at the maximum output power was hyperbolically fitted to be M_x^2~1.5 and M_y^2~1.6 along the horizontal and vertical directions, respectively, as shown in Fig. 5. The two-dimensional (2D) beam profile was recorded using an infrared camera (see the inset of Fig. 5). The pattern close to Gaussian profile validated the high beam quality operation over the entire pump power range.

3.2. Theoretical modeling and analysis

Fe:ZnSe exhibits a four-level structure and has a complementary electronic configuration with Cr:ZnSe in the tetrahedral coordination. Therefore, a rate equation to describe the population evolution of the upper laser level of Fe:ZnSe can be written as [27]:

$$\frac{dN_2(z)}{dt} = \frac{\sigma_{abs}\lambda_P I_P(z)}{hc}N_g(z) - \frac{\sigma_{ems}\lambda_L I_L(z)}{hc}N_2(z) - \frac{\sigma_{esa}\lambda_L I_L(z)}{hc}N_2(z) - \frac{N_2(z)}{\tau_f} \quad (1)$$

where $N_2(z)$ and $N_g(z)$ are the population densities of the upper laser level and ground level, respectively; σ_{abs} is the absorption cross-section at the pump wavelength (λ_P); σ_{ems} and σ_{esa} represent the emission and excited-state absorption (ESA) cross-sections at the lasing wavelength (λ_L); $I_P(z)$ is the pump intensity [$I_P(z) = I_P^+(z) + I_P^-(z)$]; $I_L(z)$ is the laser intensity [$I_L(z) = I_L^+(z) + I_L^-(z)$]; and, τ_f represents the fluorescence lifetime of the upper laser level. The population on

Optics EXPRESS

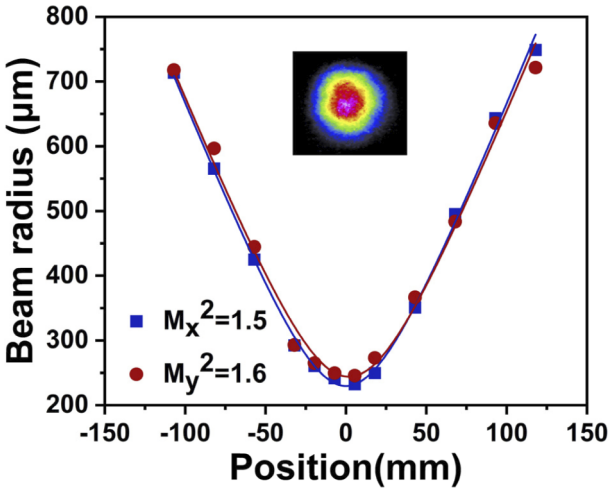

Fig. 5. Beam quality measurement at maximum output power. Inset: 2D beam profile.

the other energy levels can be reasonably neglected owing to the strong nonradiative relaxation processes. By using this approximation, we can obtain:

$$N_T(z) = N_g(z) + N_2(z) \tag{2}$$

where $N_T(z)$ represents the total doping concentration of the Fe ions. By combining Eqs. (1) and (2), the population distribution in the steady state can be solved analytically as follows:

$$N_2(z) = N_T \frac{\frac{I_P(z)}{I_{sa}}}{1 + \frac{(1+f)I_L(z)}{I_{se}} + \frac{I_P(z)}{I_{sa}}} \tag{3}$$

where I_{sa} represents the saturated absorption intensity ($I_{sa} = hc/\sigma_{abs}\lambda_P\tau_f$), I_{se} is the saturated emission intensity ($I_{se} = hc/\sigma_{ems}\lambda_L\tau_f$), and f represents the normalized ESA strength at the lasing wavelength ($f = \sigma_{esa}/\sigma_{ems}$).

It is assumed that the end facets of the Fe:ZnSe crystal are butted against the cavity mirrors such that the total intracavity loss can be lumped upon the crystal length. Additionally, a plane-wave approximation is employed for simplicity. This type of approximation is reasonable because strong interactions between the pump and laser beams only occur in the paraxial areas where the modes are highly overlapped. Therefore, a mode matching factor η was introduced to quantify the degree of overlapping between the pump mode and the cavity mode [$\eta = 4w_P^2 w_L^2 / (w_P^2 + w_L^2)^2$] [27,28], where w_P and w_L are the beam radii of the pump and cavity modes, respectively. Then the transversal variations of the pump and the cavity intensities can be neglected, and the analysis can be simplified to a one-dimensional model. The differential equations used to describe the propagation of the pump and laser intensities can be written as:

$$\frac{dI_P^{\pm}(z)}{dz} = \mp I_P^{\pm}(z) \frac{\alpha_{P0}\left[1 + \frac{(1+f)\eta I_L(z)}{I_{se}}\right]}{1 + \frac{I_P(z)}{I_{sa}} + \frac{(1+f)\eta I_L(z)}{I_{se}}} \tag{4}$$

$$\frac{dI_L^{\pm}(z)}{dz} = \pm I_L^{\pm}(z)\left[\frac{g_T(1-f)\eta\frac{I_P(z)}{I_{sa}}}{1 + \eta\frac{I_P(z)}{I_{sa}} + (1+f)\frac{I_L(z)}{I_{se}}} - \alpha_L\right] \tag{5}$$

where $I_P^+(z)$, $I_P^-(z)$, $I_L^+(z)$, and $I_L^-(z)$ are the forward and backward pump intensities and laser intensities, respectively; α_{P0} is the small signal absorption coefficient ($\alpha_{P0} = \sigma_{abs}N_T$); g_T is

Optics EXPRESS

the maximum extractable small signal gain coefficient ($g_T = \sigma_{ems} N_T$); α_L is the intracavity loss coefficient excluding the output coupling loss. The boundary conditions are given by:

$$I_P^+(0) = I_P^l \, , I_P^-(L_c) = I_P^r \, , I_L^+(0) = R_1 I_L^-(0) \, , I_L^-(L_c) = R_2 I_L^+(L_c) \tag{6}$$

where $I_P{}^l$ and $I_P{}^r$ are the average intensities of the forward and backward pump lights, respectively; R_1 and R_2 are the reflectivities of the input mirror and the output coupler, respectively; and L_c represents the crystal length. The parameters required for the calculation are based on the published spectroscopic data in conjunction with our experimental data and are summarized in Table 1.

Table 1. The parameters for the modeling of Fe:ZnSe laser

Definition	Symbol	Value/unit
Doping concentration	N_T	2.2×10^{18} cm^{-3}
Absorption cross section	σ_{abs}	1.2×10^{-18} cm^2 @2920 nm [29]
Emission cross section	σ_{ems}	2.2×10^{-18} cm^2 @4000 nm [29]
Normalized ESA coefficient	f	0.17 [30]
Fluorescence lifetime	τ_f	57 µs at 77 K [1]
Pump beam radius	w_P	140 µm
Laser beam radius	w_L	210 µm
Crystal length	L_c	8 mm
Intracavity loss coefficient	α_L	0.13 cm^{-1}
Reflectivity of input mirror	R_1	99%
Reflectivity of output coupler	R_2	80%

The laser performance can be predicted for various cavity configurations by numerically solving Eqs. (4)–(5). Figure 6(a) shows the calculated output power as a function of the absorbed pump power. Here the experimental results are shown as well for comparison. The theoretical results concur with our experimental results, proving the validity of this model in estimating the output performance of the Fe:ZnSe laser. The minor difference between the theoretical and experimental results is partially attributed to the error in the calculation of the intracavity loss owing to the lack of multiple output coupler samples, and also because the thermal effects are neglected, which will inevitably degrade the laser performance. The lasing optical efficiency was calculated as a function of the output transmission to determine the optimum transmission value. The results, shown in Fig. 6(b), indicate that an optimum output coupling transmission is ~60%, with an optical-to-optical efficiency of ~60% and an output power of ~1.5 W for 2.5 W of incident pump power. Additionally, further optimization of the output power can be achieved by increasing the crystal length to obtain a higher pump absorption, and also by modifying the cavity design to obtain better mode matching. Table 2 presents a comparison of our results with those of other reported Fe:ZnSe lasers. The Fe:ZnSe laser pumped by a 3 µm Er-doped laser only requires a two-stage pump structure, compared to those pumped by Cr-doped lasers, indicating a simpler structure and a higher wall-plug efficiency. Notably, although our experimental parameters were not optimal, the proposed Fe:ZnSe laser still achieved one of the highest optical efficiencies with a watt level of output power from a relatively low-doped Fe:ZnSe single crystal pumped by an Er:YAP laser.

The major problems hindering the power scaling in high-power laser systems are thermal effects, including thermal quenching, thermal lensing, and thermal stress-induced fracture. The thermal quenching effect for Fe:ZnSe crystals is particularly severe, such that CW lasing cannot be achieved at room temperature. Therefore, a thermal analysis of the end-pumped CW Fe:ZnSe laser was conducted by using the finite element method. Figure 7(a) shows the maximum

Optics EXPRESS

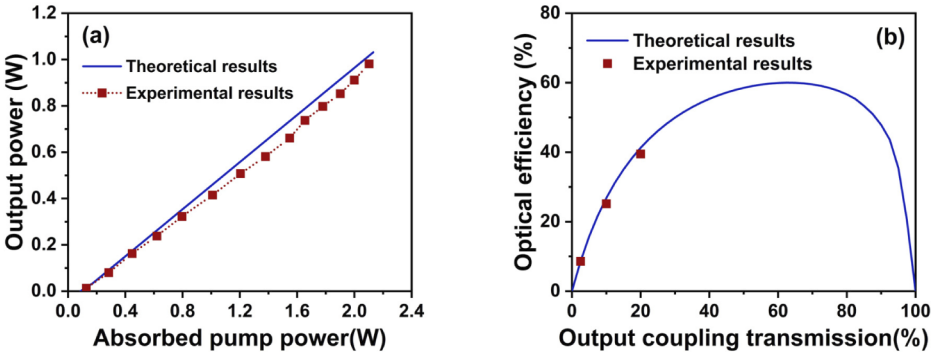

Fig. 6. (a) Calculated output power versus absorbed pump power. (b). Calculated optical efficiency versus output coupling transmission.

Table 2. Comparison of our results with other reported CW Fe:ZnSe lasers

1st-stage pump	2nd-stage pump	3rd-stage pump	Power	Efficiency[a]	Reference
LD (–)	Tm:fiber laser (3 W)	Cr:CdSe laser (0.6 W)	0.16 W	5.3%[b]	[9]
LD (–)	Er:YAG laser (2.17 W)	–	0.84 W	–	[14]
LD (27.7 W)	Er:Y_2O_3 laser (3.15 W)	–	0.42 W	1.5%	[15]
LD (–)	Tm:fiber laser (76.5 W)	Cr:ZnSe laser (23 W)	9.2 W	12%[b]	[16]
LD (35 W)	Er:ZBLAN laser (3.9 W)	–	2.1 W	6%	[17]
LD (11.4 W)	Er:YAP laser (2.5 W)	–	1.0 W	8.8%	**This work**

[a]The overall optical conversion efficiency calculated from the LD to the Fe:ZnSe laser unless otherwise noted.
[b]The optical efficiency with respect to the second-stage pump sources (Tm:fiber lasers).

temperature and thermal stress inside the Fe:ZnSe crystal as a function of the incident pump power. The maximum temperature increases with a slope of 0.55 K/W with respect to the incident pump power, while the thermal stress increases slightly with a slope of 0.03 MPa/W owing to the small thermal expansion coefficient (~1.8×10^{-6} /K at 80 K [31]) of ZnSe at cryogenic temperatures. It has been reported that the laser output power decreases rapidly when the crystal temperature exceeds 100 K [32,33], which corresponds to an incident pump power of more than 40 W based on our calculation results (see Fig. 7(a)). The maximum stress at an incident pump power of 40 W is calculated to be ~1.3 MPa, which is only 2.6% of the tensile strength of ZnSe (50 MPa), indicating the low likelihood of crystal damage. The effective thermal focal length can be given by [34]:

$$f_{th} = \frac{\pi K_c w_P^2}{P_p \gamma (dn/dT)} \left[\frac{1}{1 - \exp(-\alpha_P L_c)} \right] \tag{7}$$

where K_c represents the thermal conductivity (~1.03 W/cm·K at 80 K [35]), P_p is the incident pump power, γ is the fraction of the absorbed pump power that converted to heat (52% in our case), and dn/dT is the thermo-optic coefficient (~4.7×10^{-5} /K at 4 μm at 80 K [36]). Figure 7(b) shows a plot of the calculated values for the effective thermal focal length as a function of the incident pump power. The thermal lensing effect is observed to be relatively strong owing to the large thermo-optic coefficient of the ZnSe material. In our experimental configuration, the minimum thermal focal length which prevents a significant mode distortion is ~11 mm, corresponding to a maximum tolerable incident pump power of ~27 W. Based on this pump power and the rate equation model presented above, a CW output power of more than 11 W is expected with the use of an improved pump source in the future.

Optics EXPRESS

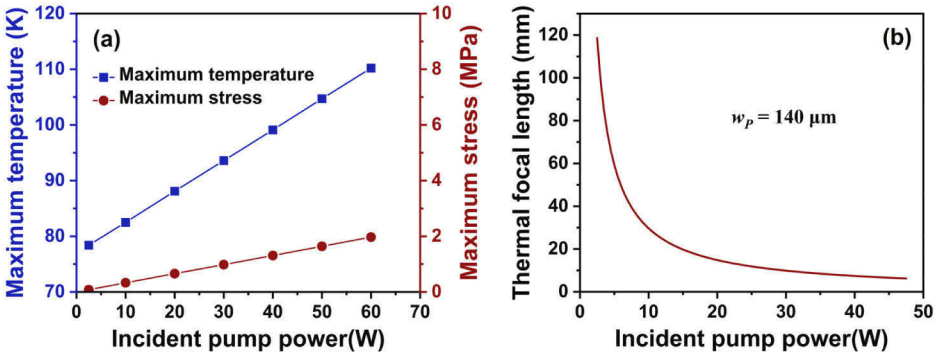

Fig. 7. (a) The maximum temperature and thermal stress versus incident pump power. (b) Thermal focal length versus incident pump power for 140 μm pump radius.

4. Conclusions

In conclusion, this study presents a high-efficiency CW Fe:ZnSe mid-IR laser end pumped by a self-constructed Er:YAP laser operating at 2920 nm. The compact Er:YAP laser generated a stable output power of 3.6 W with an average slope efficiency of 36.6%. The Fe:ZnSe laser produced an output power of approximately 1 W with a good beam quality ($M^2 < 1.6$) at an absorbed pump power of 2.1 W, corresponding to an average slope efficiency of 48% and an optical-to-optical efficiency of 40%. The overall optical conversion efficiency, calculated from the 976 nm diode laser to the 4 μm Fe:ZnSe laser, was 8.8%, which is the highest value reported thus far. These results indicate that the Er:YAP laser can be a reliable pump source for the Fe:ZnSe laser, owing to its high performance, low cost, and power scalable properties. Additionally, this study presents a theoretical model of the CW Fe:ZnSe laser to predict the optimized laser performance. The results indicate that there is considerable scope for further improvement in the power performance by increasing the output coupling transmission to ~60% and by employing a relatively longer Fe:ZnSe crystal to absorb a greater fraction of the pump light. The numerical thermal analysis demonstrates that the thermal lensing effect is crucial in hindering the power scaling of the Fe:ZnSe laser. To the best of our knowledge, this is the first study that combines experiment and theoretical analysis in a CW Fe:ZnSe laser system. We believe that the theoretical model presented in this study is expected to provide a rough guide for scaling the power levels of the CW Fe:ZnSe lasers to the order of tens of watts in future studies.

Funding. Japan Society for the Promotion of Science (18H01204, 20K05374, 21H01845); JSPS Bilateral Joint Research Project (JPJSBP120214808); Russian Foundation for Basic Research (21-52-50005); Amada Foundation (AF-2019221-B3, AF-2020228-B3); National Institutes of Natural Sciences (01312106); Research Foundation for Opto-Science and Technology; National Institute for Fusion Science (KLEH082).

Disclosures. The authors declare no conflicts of interest.

Data availability. Data underlying the results presented in this paper are not publicly available at this time, but may be obtained from the authors upon reasonable request.

References

1. S. B. Mirov, I. S. Moskalev, S. Vasilyev, V. Smolski, V. V. Fedorov, D. Martyshkin, J. Peppers, M. Mirov, A. Dergachev, and V. Gapontsev, "Frontiers of Mid-IR Lasers Based on Transition Metal Doped Chalcogenides," IEEE J. Sel. Top. Quantum Electron. **24**(5), 1–29 (2018).
2. M. Ebrahim-Zadeh and I. T. Sorokina eds, "Mid-infrared coherent sources and applications," *NATO Science for Peace and Security, Series B: Physics and Biophysics*. (Springer Verlag, The Netherlands, 2008).
3. P. Fjodorow, M. P. Frolov, Y. V. Korostelin, V. I. Kozlovsky, C. Schulz, S. O. Leonov, and Y. K. Skasyrsky, "Room-temperature Fe:ZnSe laser tunable in the spectral range of 3.7-5.3 μm applied for intracavity absorption spectroscopy of CO_2 isotopes, CO and N_2O," Opt. Express **29**(8), 12033–12048 (2021).

Optics EXPRESS

4. B. M. Walsh, H. R. Lee, and N. P. Barnes, "Mid infrared lasers for remote sensing applications," J. Lumin. **169**, 400–405 (2016).
5. V. I. Kozlovsky, Y. V. Korostelin, Y. P. Podmar'kov, Y. K. Skasyrsky, and M. P. Frolov, "Middle infrared Fe^{2+}:ZnS, Fe^{2+}:ZnSe and Cr^{2+}:CdSe lasers: new results," J. Phys.: Conf. Ser. **740**, 012006 (2016).
6. Y. Li, L. Xu, Y. Ju, B. Yao, and T. Dai, "Free-running Fe:ZnSe laser pumped by an Er:YAG radiation along the cavity axis," Optik **194**, 162949 (2019).
7. D. V. Martyshkin, V. V. Fedorov, M. Mirov, I. Moskalev, S. Vasilyev, and S. B. Mirov, "High average power (35 W) pulsed Fe:ZnSe laser tunable over 3.8-4.2 µm," in *CLEO: 2015*, (Optical Society of America, 2015), OSA Technical Digest (online), p. SF1F.2.
8. K. Karki, S. Yu, V. Fedorov, D. Martyshkin, S. Subedi, Y. Wu, and S. Mirov, "Hot-pressed ceramic Fe:ZnSe gain-switched laser," Opt. Mater. Express **10**(12), 3417–3423 (2020).
9. A. A. Voronov, V. I. Kozlovsky, Yu. V. Korostelin, A. I. Landman, Yu. P. Podmar'kov, Ya. K. Skasyrsky, and M. P. Frolov, "A continuous-wave Fe^{2+}:ZnSe laser," Quantum Electron. **38**(12), 1113–1116 (2008).
10. J. W. Evans, P. A. Berry, and K. L. Schepler, "A Passively Q-Switched, CW-Pumped Fe:ZnSe Laser," IEEE J. Quantum Electron. **50**(3), 204–209 (2014).
11. V. Fedorov, D. Martyshkin, K. Karki, and S. Mirov, "Q-switched and gain-switched Fe:ZnSe lasers tunable over 3.60–5.15 µm," Opt. Express **27**(10), 13934–13941 (2019).
12. H. Uehara, T. Tsunai, B. Han, K. Goya, R. Yasuhara, F. Potemkin, J. Kawanaka, and S. Tokita, "40 kHz, 20 ns acousto-optically Q-switched 4 µm Fe:ZnSe laser pumped by fluoride fiber laser," Opt. Lett. **45**(10), 2788–2791 (2020).
13. A. V. Pushkin, E. A. Migal, S. Tokita, Y. V. Korostelin, and F. V. Potemkin, "Femtosecond graphene mode-locked Fe:ZnSe laser at 4.4 µm," Opt. Lett. **45**(3), 738–741 (2020).
14. J. W. Evans, P. A. Berry, and K. L. Schepler, "840 mW continuous-wave Fe:ZnSe laser operating at 4140 nm," Opt. Lett. **37**(23), 5021–5023 (2012).
15. J. W. Evans, T. Sanamyan, and P. A. Berrya, "A continuous-wave Fe:ZnSe laser pumped by an efficient Er:Y_2O_3 laser," Proc. SPIE **9342**, 93420F (2015).
16. D. V. Martyshkin, V. V. Fedorov, M. Mirov, I. Moskalev, S. Vasilyev, V. Smolski, A. Zakrevskiy, and S. B. Mirov, "High Power (9.2 W) CW 4.15 µm Fe:ZnSe laser," in *Conference on Lasers and Electro-Optics*, OSA Technical Digest (online) (Optical Society of America, 2017), STh1L.6.
17. A. V. Pushkin, E. A. Migal, H. Uehara, K. Goya, S. Tokita, M. P. Frolov, Y. V. Korostelin, V. I. Kozlovsky, Y. K. Skasyrsky, and F. V. Potemkin, "Compact, highly efficient, 2.1 W continuous-wave mid-infrared Fe:ZnSe coherent source, pumped by an Er:ZBLAN fiber laser," Opt. Lett. **43**(24), 5941–5944 (2018).
18. I. Moskalev, S. Mirov, M. Mirov, S. Vasilyev, V. Smolski, A. Zakrevskiy, and V. Gapontsev, "140 W Cr:ZnSe laser system," Opt. Express **24**(18), 21090–21104 (2016).
19. S. Tokita, M. Murakami, and S. Shimizu, "High Power 3 µm Erbium Fiber Lasers," in *Advanced Solid State Lasers*, OSA Technical Digest (online) (Optical Society of America, 2014), AM3A.4.
20. W. Yao, H. Uehara, H. Kawase, H. Chen, and R. Yasuhara, "Highly efficient Er:YAP laser with 6.9 W of output power at 2920 nm," Opt. Express **28**(13), 19000–19007 (2020).
21. J. Koetke and G. Huber, "Infrared excited-state absorption and stimulated-emission cross sections of Er^{3+}-doped crystals," Appl. Phys. B **61**(2), 151–158 (1995).
22. T. Li, K. Beil, C. Kränkel, and G. Huber, "Efficient high-power continuous wave Er:Lu_2O_3 laser at 2.85 µm," Opt. Lett. **37**(13), 2568–2570 (2012).
23. C. Quan, D. Sun, J. Luo, H. Zhang, Z. Fang, X. Zhao, L. Hu, M. Cheng, Q. Zhang, and S. Yin, "2.7 µm dual-wavelength laser performance of LD end-pumped Er:YAP crystal," Opt. Express **26**(22), 28421–28428 (2018).
24. A. A. Voronov, V. I. Kozlovskii, Yu. V. Korostelin, A. I. Landman, Yu. P. Podmar'kov, and M. P. Frolov, "Laser parameters of a Fe:ZnSe laser crystal in the 85-255K temperature range," Quantum Electron. **35**(9), 809–812 (2005).
25. D. Findlay and R. A. Clay, "The measurement of internal losses in 4-level lasers," Phys. Lett. **20**(3), 277–278 (1966).
26. J. W. Evans, T. R. Harris, B. R. Reddy, K. L. Schepler, and P. A. Berry, "Optical spectroscopy and modeling of Fe^{2+} ions in zinc selenide," J. Lumin. **188**, 541–550 (2017).
27. A. Sennaroglu, A. Ozgun Konca, and C. R. Pollock, "Continuous-wave power performance of a 2.47-µm Cr^{2+}:ZnSe laser: Experiment and modeling," IEEE J. Quantum Electron. **36**(10), 1199–1205 (2000).
28. A. Sennaroglu, "Optimum crystal parameters for room-temperature Cr^{4+}:forsterite lasers: experiment and theory," Opt. Commun. **174**(1-4), 215–222 (2000).
29. J. W. Evans, R. W. Stites, and T. R. Harris, "Increasing the performance of an Fe:ZnSe laser using a hot isostatic press," Opt. Mater. Express **7**(12), 4296–4303 (2017).
30. H. Cankaya, U. Demirbas, A. K. Erdamar, and A. Sennaroglu, "Absorption saturation analysis of Cr^{2+}:ZnSe and Fe^{2+}:ZnSe," J. Opt. Soc. Am. B **25**(5), 794–800 (2008).
31. J. S. Browder and S. S. Ballard, "Low temperature thermal expansion measurements on optical materials," Appl. Opt. **8**(4), 793–798 (1969).
32. J. W. Evans, P. A. Berry, and K. L. Schepler, "A broadly tunable continuous-wave Fe:ZnSe laser," Proc. SPIE **8599**, 85990C (2013).
33. Y. Y. Li, K. Yang, G. Y. Liu, L. W. Xu, B. Q. Yao, Y. L. Ju, T. Y. Dai, and X. M. Duan, "A 1 kHz Fe:ZnSe Laser Gain-Switched by a $ZnGeP_2$ Optical Parametric Oscillator at 77 K," Chin. Phys. Lett. **36**(7), 074201 (2019).

Optics EXPRESS

34. M. E. Innocenzi, H. T. Yura, C. L. Fincher, and R. A. Fields, "Thermal modeling of continuous-wave end-pumped solid-state lasers," Appl. Phys. Lett. **56**(19), 1831–1833 (1990).
35. G. Slack, "Thermal Conductivity of II-VI Compounds and Phonon Scattering by Fe^{2+} Impurities," Phys. Rev. B **6**(10), 3791–3800 (1972).
36. D. B. Leviton, B. J. Frey, and T. Kvamme, "High accuracy, absolute, cryogenic refractive index measurements of infrared lens materials for JWST NIRCam using CHARMS," Proc. SPIE **5904**, 59040O (2005).